Surface & Coatings Technology 349 (2018) 1077–1082

Contents lists available at ScienceDirect

Surface & Coatings Technology

journal homepage: www.elsevier.com/locate/surfcoat

Tribocorrosion behavior of TiO_2/Al_2O_3 nanolaminate, Al_2O_3, and TiO_2 thin films produced by atomic layer deposition

Polyana Alves Radi[a,b,*], Giorgio Ernesto Testoni[c], Rodrigo Sávio Pessoa[a,b], Homero Santiago Maciel[a,b], Luís Augusto Rocha[d,e,f], Lucia Vieira[a,b]

[a] Plasma and Processes Laboratory, Aeronautics Institute of Technology (ITA), Centro de Ciência e Tecnologia de Plasmas e Materiais (PlasMat), Sao Paulo, Brazil
[b] Nanotechnology and Plasmas Processes Laboratory (NanoTecPlasma), University of Paraíba Valley (UNIVAP), São José dos Campos, Sao Paulo, Brazil
[c] University Center SOCIESC - UNISOCIESC, Joinville, Santa Catarina, Brazil
[d] São Paulo State University (UNESP), Faculty of Sciences of Bauru, Physics Department, Bauru, Sao Paulo, Brazil
[e] Brazilan Branch of the Institute of Biomaterials, Tribocorrosion and Nanomedicine (IBTN/Br), Bauru, Sao Paulo, Brazil
[f] Center for MicroElectroMechanical Systems (CMEMS), Universidade do Minho, Azurém, Guimarães, Portugal

ARTICLE INFO

Keywords:
ALD
Tribocorrosion
Nanolaminates
Al_2O_3
TiO_2
Tribology

ABSTRACT

Metallic materials are the most widely used for orthopedic applications and, their corrosion resistance is one of the main prerequisites for avoiding impairment of the material properties due to degradation. Ti-6Al-4V is one of the main medical titanium alloys. However, for permanent implant applications, this alloy may cause toxic effect due to release of vanadium and aluminum. Nanolaminates of alternatively ordered thin films of transition metal oxides with nanoscale thickness are known to have distinct properties of a single layer film. Atomic layer deposition (ALD) is a promising method for fabrication of thin sealing coatings for corrosion protection. These films can also be used as *in vivo* sensors to antedate the detection of diseases such as cancer, to inform the best treatments, and to understand the response to therapies. The ideal *in vivo* sensor should be non-toxic, biocompatible, stable, and very sensitive. In this work, TiO_2/Al_2O_3 nanolaminate, Al_2O_3 and TiO_2 thin films were deposited on Ti-6Al-4V substrates by using ALD and their structure, adhesion and tribocorrosion properties were analyzed. The tribocorrosion tests were performed in Ringer's solution. The coatings showed to protect the sample surface evidenced by the increase on the OCP both in static mode and in dynamic mode. The TiO_2/Al_2O_3 nanolaminates presented lower friction coefficient.

1. Introduction

The human body is an aqueous medium containing ions and organic substances, pH ~ 7.4, and temperature of 37 ± 1 °C [1, 2]. Within the body, corrosion and wear resistance are significant prerequisites to avoid material degradation, because corrosive products or abrasive particles can damage the host tissue [3, 4]. In a corrosive environment, it is complex to predict the tribological behavior considering both wear and corrosion, because their synergistic or antagonistic effects can accelerate or slow-down the wear process [5–7]. The combined action of corrosion and wear on a material is defined as tribocorrosion [5, 8, 9]. This emerging research area is very relevant in the study of materials for chemical, marine, aerospace [10], automotive, and biomedical applications [5].

Metals and their alloys are essential on the orthopedic area and the basic requirements for a successful application of an implant are chemical stability, proper mechanical behavior, and biocompatibility with body fluids and tissues [1, 11]. Ti-6Al-4V alloy is among the most corrosion and mechanical resistant materials used for implants. Nevertheless, in the body, it can corrode and release titanium, aluminum, and vanadium that can cause poisoning and certain diseases, which can be aggravated with implant fretting and subsequent fracture [1, 12]. The deposition of corrosion resistant films on Ti-6Al-4V prosthesis can increase biocompatibility, reduce friction, wear, and corrosion, thereby avoiding the release of titanium alloy constituents [1].

The atomic layer deposition (ALD) technique allows depositing a variety of thin film materials from the vapor phase with exceptional conformity on high-aspect-ratio structures, thickness control at the angstrom level, and tunable film composition. Due to this, ALD has emerged as a powerful tool for many industrial and research applications and can be used in biomedical area, for example, in functionalized pharmaceuticals or implanted detectors. Also, ALD can be used to produce super durable coatings with good tribological behavior, on various surfaces, as well as many others that can benefit from its unique

* Corresponding author at: Av. Shishima Hifumi, 2911 - Urbanova, IP&D, sala 44, São José dos Campos, SP 12244-000, Brazil.
E-mail address: polyana@ita.br (P.A. Radi).

https://doi.org/10.1016/j.surfcoat.2018.06.036
Received 24 March 2018; Received in revised form 16 June 2018; Accepted 20 June 2018
Available online 20 June 2018
0257-8972/ © 2018 Elsevier B.V. All rights reserved.

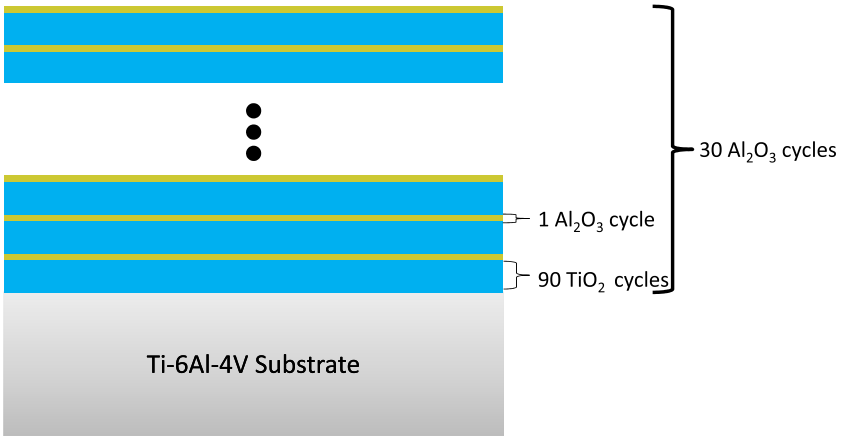

Fig. 1. Schematic drawn of the TiO_2/Al_2O_3 nanolaminate design prepared for this study.

Table 1
Composition and ionic concentration of Ringer's solution.

Composition (g/L)		Ionic concentration (mEq/L)	
Sodium chloride (NaCl)	8.60	Na^+	147.16
Potassium chloride (KCl)	0.30	Ca^{-2}	4.49
Calcium chloride ($CaCl_2$)	0.33	Cl^-	155.67
Water	q.s.	K^+	4.02

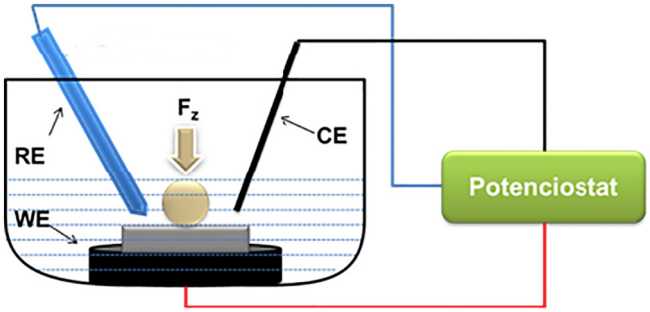

Fig. 2. Schematic drawing of tribocorrosion cell showing the reference electrode (RE) Ag/AgCl, the platinum counter electrode (CE) and the working electrode (WE).

and precise control over thickness and composition [13].

Titanium dioxide (TiO_2) is a promising biomaterial mainly because it becomes sterile when rightly stimulated by ultraviolet radiation. The alumina (Al_2O_3) offers the advantage of bio-inertness, although it is not as sterile as TiO_2. However, Al_2O_3 mixed with TiO_2 in the form of nanolaminate will allow the control of the degree of porosity of the ceramic ensuring new potential applications [14]. This nanolaminate is expected to exhibit high Young's modulus which is of great interest for micro- and nano-electromechanical devices [15]. It can also be applied as *in vivo* sensor to dynamically and continuously monitor biological processes helping to antedate the diagnosis of diseases such as cancer, to inform about treatments and to help understanding responses to therapies [16, 17]. Similar to the orthopedic implants, the *in vivo* sensors must be non-toxic, biocompatible, relatively stable and additionally very sensitive [16].

In this paper, TiO_2/Al_2O_3 nanolaminates, Al_2O_3 and TiO_2 thin films were deposited on Ti-6Al-4V substrates using ALD technique, and the films structure, adhesion and tribocorrosion properties were analyzed. An Al_2O_3 top layer was used on TiO_2/Al_2O_3 nanolaminates to improve the resistance to corrosion of the film and reduces the friction coefficient.

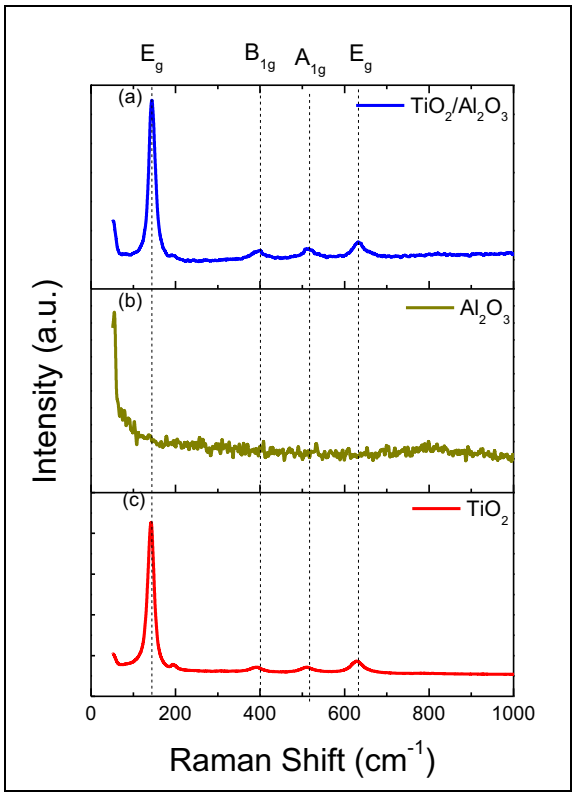

Fig. 3. Micro-Raman spectra of the (a) TiO_2/Al_2O_3 nanolaminate, (b) Al_2O_3 and (c) TiO_2 films deposited on Ti-6Al-4V substrates.

2. Experimental

2.1. Synthesis of Al_2O_3, TiO_2 and TiO_2/Al_2O_3 films

TiO_2/Al_2O_3, Al_2O_3 and TiO_2 films were deposited by a TFS-200 ALD system from Beneq. The reaction chamber is a low-volume cross flow type operating in thermal mode. Ti-6Al-4V pieces ($2.0 \times 2.0\ cm^2$) and Si wafer (p-type, $5 \times 10^{-3}\ \Omega$ cm, (100)-orientation) were used as substrates.

Prior to the deposition, the substrates were individually cleaned in an ultrasonic bath using acetone for 10 min and then dried under N_2 gas flow. The nanolaminate was constructed by alternating 90 cycles of TiO_2 and 1 cycle of Al_2O_3 in supercycle until complete 30 supercycles or 30 Al_2O_3 layers as demonstrated in Fig. 1. The first stage of the nanolaminate was 90 layers of TiO_2 and the film top layer was composed by

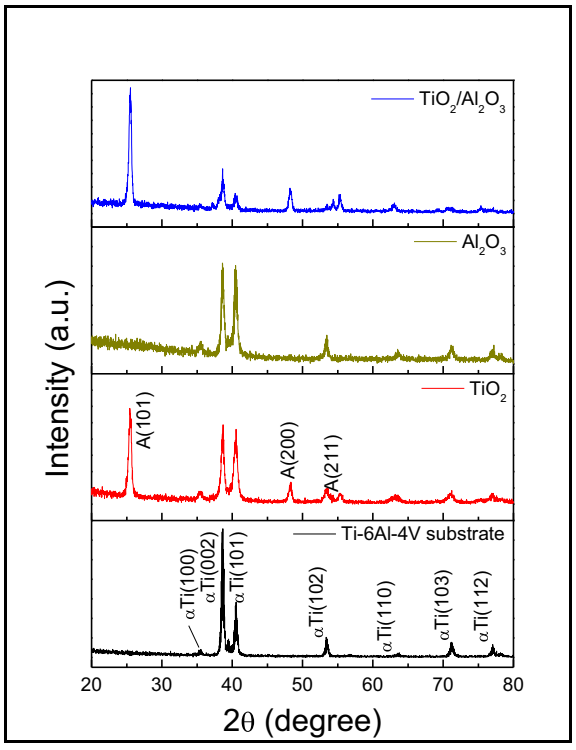

Fig. 4. GIXRD spectra of the (a) TiO_2/Al_2O_3 nanolaminate, (b) Al_2O_3 film, (c) TiO_2 film and (d) bare Ti-6Al-4V substrate.

Al_2O_3 in order to provide better resistance to corrosion. Details concerning the TiO_2/Al_2O_3 nanolaminate film can be found in previous work [15]. Titanium tetraisopropoxide (TTIP, ⩾97%, Sigma-Aldrich) and trimethylaluminum (TMA, 97%, Sigma-Aldrich) were used as Ti and Al precursors, respectively. The deionized water, used as oxygen reagent, was stored in a vessel at room temperature. The TTIP precursor and vapor delivery line were heated at 70 °C to avoid precursor condensation. High purity nitrogen (N_2, 99.999%) was used as purge as well as carrier gas for the TTIP precursor. The base pressure of the reactor was below 10^{-2} mbar and the gas pressure was kept around 1.0 mbar during the deposition, through insertion of N_2 at 300 sccm gas flow. The process temperature was of about 250 ± 3 °C for all films. The films structures were analyzed by Raman spectroscopy and X-ray diffractometry. For Raman analysis, a confocal Raman microscope from Horiba- Model Lab Ram HR Evolution with laser wavelength (λ = 532 nm) was used. Here the calibration of the peaks was performed using a diamond peak. GIXRD patterns were obtained at room temperature in a Shimadzu XRD 6000 goniometer using a copper target (CuKα radiation 1.5418 Å), 2θ from 20 °C–80 °C, at a scanning speed of $0.02^\circ\,s^{-1}$, a voltage of 40 kV, a current of 30 mA, and an incidence angle of 0.29° [18].

2.2. Adherence tests

The adherence of the films was evaluated according to VDI 3198 indentation test evaluation and by micro-scratching test [19]. The VDI 3198 indentation test is a Rockwell C indentation on planar surfaces of coated compounds. This test enables to evaluate the film adhesion, cohesion and its brittleness. The VDI 3198 was performed using a Rockwell C diamond tip with curvature radius of 200 μm and a weight of 150 kg. The contact geometry combined with the high load transfer induces extreme shear stresses at the interface [20]. The indentation mark was analyzed by using SEM (Scanning Electron Microscopy) and, the failure of the films was classified as acceptable and unacceptable.

Micro-scratch tests were conducted on the sample surfaces using a diamond stylus (Rockwell C 120°) with a 200 μm radius diamond tip to evaluate the adherence between the film and the substrate. A progressive load (0–30 N) at a constant load rate (0.3 N/s) was applied over 10 mm length at 0.1 mm/s. Friction coefficient and acoustic emission were measured for each test and the same test parameters were used for a given set of samples. The tests were performed in triplicate. The critical load (LcN) was evaluated according to the type of damage observed on scratch track, which were categorized according to ASTM C1624-05 [19]. The first critical normal load (LC1), is related to the first damages or cracks on the films and are evidenced by the rise in the acoustic emission; The second critical load (LC2), is related to the complete coating failure [21–23] and are evidenced by a sudden change on the friction coefficient.

Additionally, hardness tests were performed using a Hysitron Ti950 triboindenter using a Berkovich indenter. The experimental setup for hardness evaluation was under a max load of 10 mN at 9 points from each sample to obtain an average. The distance between indentations was 15 μm, based on Oliver and Pharr method [24] and the penetration depth was about 10% of the film thickness.

2.3. Tribocorrosion tests

Tribocorrosion tests were conducted on bare Ti-6Al-4V and Ti-6Al-4V covered with Al_2O_3, TiO_2 and TiO_2/Al_2O_3 films using a Bruker tribometer on reciprocating conditions at tribocorrosion set in Ringer's solution based on ASTM G119-93 [6]. The Ringers solution pH was maintained between 5.0 and 7.5. Its composition and ionic concentration are presented in Table 1.

The open circuit potentials (OCPs) were measured for 60 min before and after tribocorrosion tests, to verify the thermodynamic tendency for corrosion [25]. The oscillation frequency of the pin was controlled at 1 Hz under an applied normal load of 1 N (4.2 GPa Hertzian initial contact pressure) and a stroke length of 2 mm. An alumina ball with 4.76 mm diameter was used as counter-body with a fresh surface on each test. A three-electrode electrochemical cell configuration was used

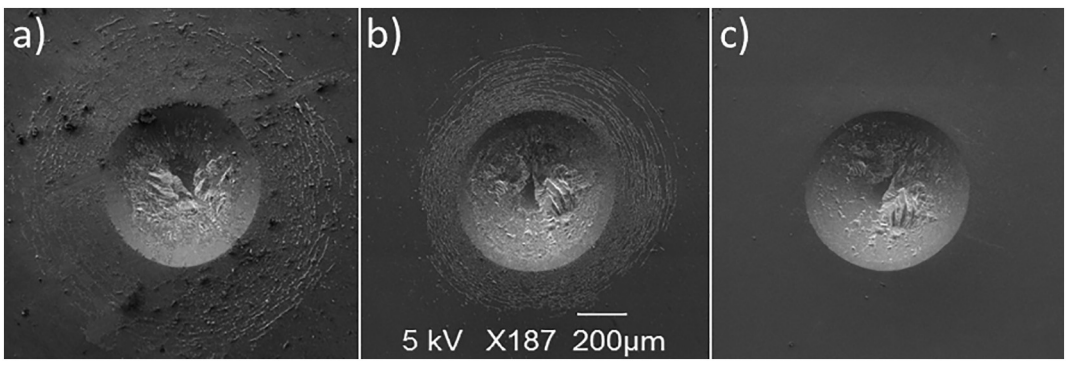

Fig. 5. SEM images showing the indentation marks performed on (a) TiO_2/Al_2O_3 nanolaminate, (b) Al_2O_3, and (c) TiO_2 films, according to VDI 3198 [20].

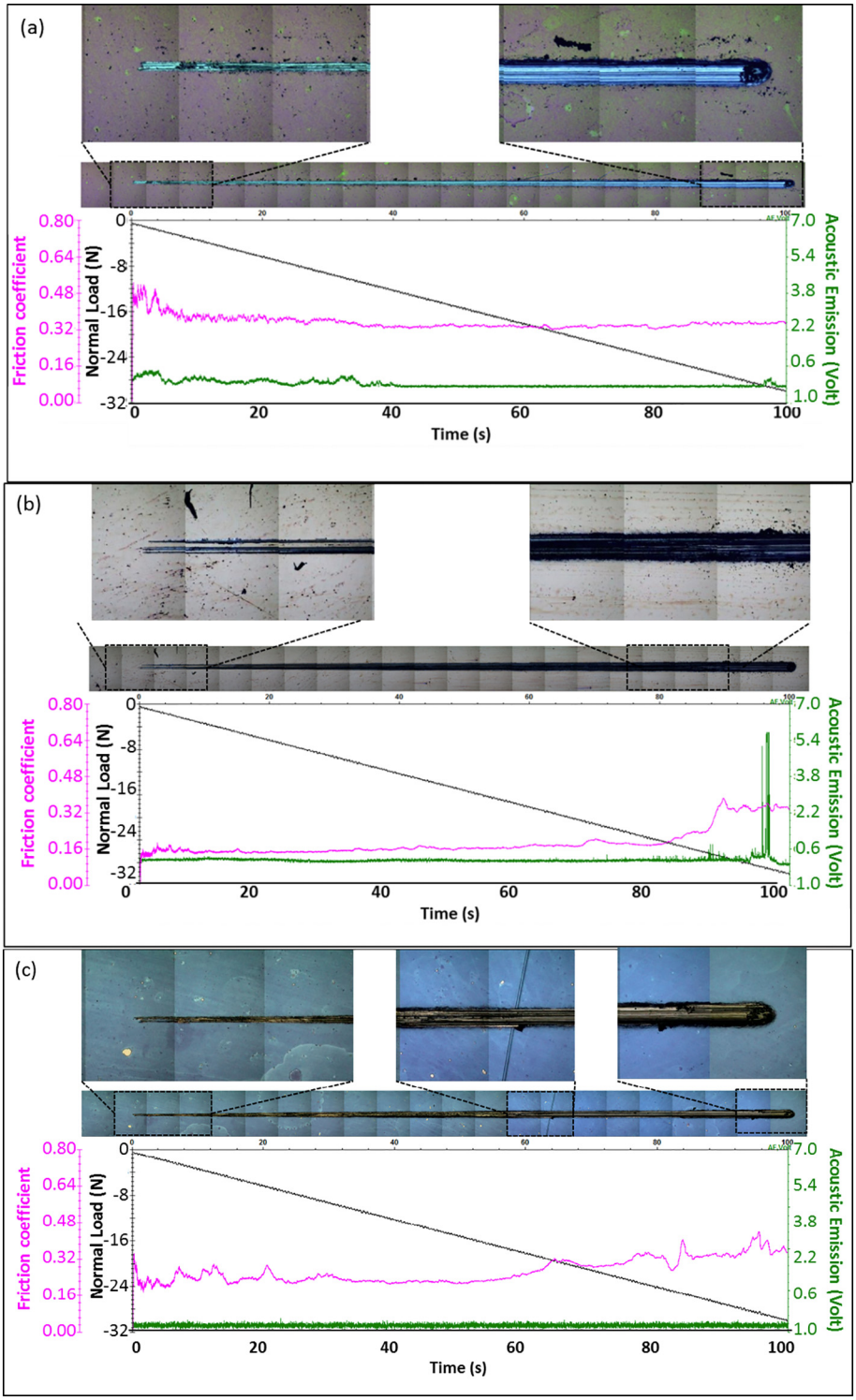

Fig. 6. Applied load (Fz, black line), friction coefficient (COF - pink), and acoustic emission (AE, green) *versus* time (s) and track image for scratching test on (a) TiO_2/Al_2O_3 (b) Al_2O_3, and (c) TiO_2 films. The scratched track image was obtained by optical microscopy. (For interpretation of the references to color in this figure, the reader is referred to the web version of this article.)

with a platinum wire counter electrode and an Ag/AgCl (3 M KCl) reference electrode. The area in contact with the electrolyte was of 1.50 cm^2. The OCPs were measured for 60 min before the start of sliding to allow its stabilization. The tribocorrosion test was carried out for 30 min and upon stopping the tribological contact, the OCP was measured for an additional 60 min to investigate repassivation. The tests were performed three times for each sample. Fig. 2 shows the schematic drawing from the tribocorrosion cell with the reference electrode (RE) Ag/AgCl and platinum counter electrode (CE) and working electrode (WE). The results were analyzed according to ASTM G3-14 [26].

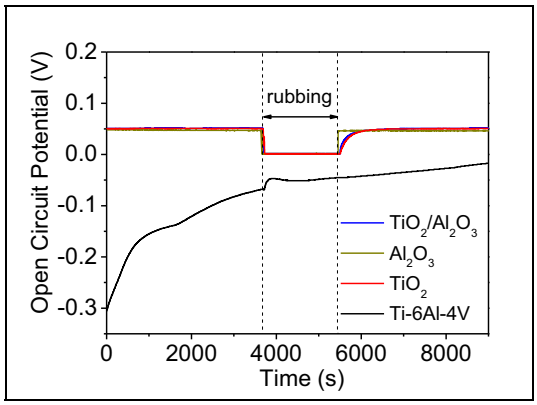

Fig. 7. Evolution of open circuit potential (OCP *vs* Ag/AgCl) values before, during and after tribocorrosion tests using alumina ball against the following samples: bare Ti-6Al-4V, and Ti-6Al-4V covered with TiO_2/Al_2O_3, Al_2O_3 or TiO_2, in Ringer's solution at room temperature.

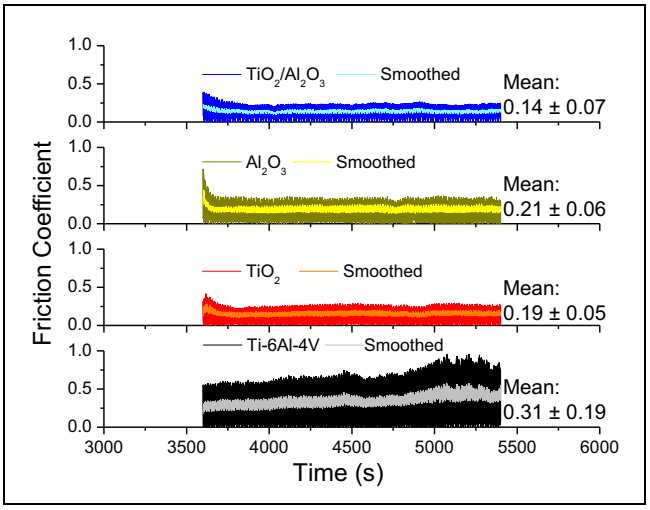

Fig. 8. Friction coefficient results obtained during tribocorrosion test using alumina ball against bare and Al_2O_3, TiO_2 and TiO_2/Al_2O_3 covered Ti-6Al-4V.

3. Results and discussion

3.1. Raman and GIXRD analyzes

Fig. 3 shows the Raman spectra of the (a) TiO_2/Al_2O_3, (b) Al_2O_3 and (c) TiO_2 films. Al_2O_3 films exhibits the very weak Raman bands due to the low polarizability of light atoms and the ionic character of the Al—O bonds [27]. On the other hand, for the TiO_2/Al_2O_3 nanolaminate and TiO_2 films (Fig. 3a and c) four Raman-active modes associated to anatase structure were observed: A_{1g} (519 cm^{-1}), B_{1g} (397 cm^{-1}) and E_g (144 and 636 cm^{-1}) with an intense peak at 144 cm^{-1}.

Fig. 4 presents the GIXRD patterns of the (a) TiO_2/Al_2O_3 nanolaminate, (b) Al_2O_3 film, (c) TiO_2 film and (d) bare Ti-6Al-4V substrate. The results corroborate with those of Raman, evidencing the presence of the anatase phase for the TiO_2 and TiO_2/Al_2O_3 films and the amorphous structure of the Al_2O_3 film. Additionally, the spectrum of the bare-Ti-6Al-4V substrate (Fig. 4d) is shown, confirming the α-structure of the Ti alloy [27]. From this spectrum, the presence of the substrate signal in the ALD covered-samples was observed. This fact is due to thin thickness of the films: 355 nm Al_2O_3, 100 nm TiO_2 and 85 nm TiO_2/Al_2O_3 [15].

3.2. Adhesion and hardness

The adhesion of the films was evaluated using the VDI 3198 standard test [20] and the failure was classified as acceptable and unacceptable. The indentation marks in Fig. 5 show that all films presented acceptable failures according to the standard, as no substrate exposition was observed. The TiO_2/Al_2O_3 nanolaminate (Fig. 5a) and Al_2O_3 (Fig. 5b) presented radial cracks around the indentation mark indicating brittleness but high adhesion to the substrate. The TiO_2 film (Fig. 5c) presented better adhesion as no crack or delamination was observed around the indentation mark. Following the VDI 3198 standard, the Al_2O_3 and TiO_2/Al_2O_3 films demonstrated HF3 level, while the TiO_2 film HF1.

The resistance of the films was evaluated by scratch test, and the results are presented in Fig. 6 with the optical images from the scratched track. In addition, the plots of the friction coefficient (COF) (pink line), the normal load (FN) (black line), and acoustic emission (green line) as a function of time are presented in Fig. 6 for (a) Al_2O_3 (b) TiO_2 and (c) TiO_2/Al_2O_3 nanolaminates. The plastic deformation of the Ti-6Al-4V substrate is the main cause of the coating failure, because the coating follows the substrate deformation until the point where the tensile stress inside and at the interface of the coating leads to cracking and delamination of the film [28]. The first critical normal load, LC_1, was related to the first damages or cracks on the films and was evidenced by the rise in the acoustic emission. The second critical load, LC_2, was related to the complete coating failure. Fig. 6(a) shows the scratching test results for Al_2O_3 film and is possible to see some lateral cracks on the beginning of the track but the film remains on the track keeping low friction coefficient until 27 N. The film failure was evidenced by the increase on the friction coefficient and by the acoustic emission signal. Concerning to Fig. 6(b), similar to Al_2O_3, the TiO_2 film presented some lateral cracks from the start of the track but the friction remained low until 20 N when the film failed completely, and the friction coefficient increased to around 0.32. The TiO_2/Al_2O_3 nanolaminate (Fig. 6c) failure at the beginning of the track was evidenced by the optical images from the track and the friction coefficient that was around 0.4 since the beginning of the test. This lower resistance to scratch can be attributed to crystallization of TiO_2 grains on the film structure as showed by Testoni et al. [15]. More details about failure modes can be found in ASTM C1624-05 [19].

The nanohardness of the films was evaluated and was 8.08 ± 1.6 GPa for TiO_2/Al_2O_3, 9.76 ± 0.22 GPa for Al_2O_3, 6.86 ± 0.78 GPa for TiO_2. The nanolaminate presented intermediate hardness compared with Al_2O_3 and TiO_2.

3.3. Tribocorrosion

The tribocorrosion was evaluated through the evolution of OCP on static and dynamic mode. Fig. 7 shows the evolution of OCP before, during and after tribocorrosion tests on bare Ti-6Al-4V and covered with Al_2O_3, TiO_2 and TiO_2/Al_2O_3 films immersed in Ringer's solution at room temperature. In the Ti-6Al-4V sample, was possible to observe an increase of the OCP before the start of sliding, which can be attributed to the growth of the passive film. All coated samples presented higher OCP values (about +0.5 V) before tribocorrosion test and around 0 V during tribocorrosion test. After the tribocorrosion test, the OCP of Al_2O_3 film recovered instantly while for TiO_2/Al_2O_3 nanolaminate and TiO_2 film the recovery was gradual. The recovery of the OCP at the end of the movement indicates that the newly formed passive film, together with the mixed mechanical layer has quite similar characteristics as the naturally formed film before the sliding [29]. After the tribocorrosion the tracks were analyzed but it could not be found and no wear could be detected for all covered samples.

Fig. 8 shows the friction coefficient results obtained during tribocorrosion tests using alumina ball against bare and covered Ti-6Al-4V. Samples with the thin films had a friction coefficient lower than that

recorded for the Ti6Al4V samples (~0.31). The TiO_2/Al_2O_3 nanolaminate presented the lowest friction coefficient (~0.14). These results indicate that the TiO_2/Al_2O_3 nanolaminate film is a promising top coating with low friction coefficient. Nevertheless, the results from the scratch test suggest that the films are indicated for use in low load applications, such those that can be expected for a dispositive used for implanted sensors.

4. Conclusion

In this paper, the tribocorrosion behavior of bare Ti-6Al-4V and Al_2O_3, TiO_2 and TiO_2/Al_2O_3 covered Ti-6Al-4V was investigated in Ringer's solution for static and dynamic modes under 1 N, 1 Hz at reciprocating conditions. The Al_2O_3 film presented higher L_{c2} (~27 N), followed by TiO_2 (~20 N) and TiO_2/Al_2O_3 (~1 N). All films improved the tribocorrosion and tribological behavior in relation to the Ti-6Al-4V sample. All films reduced the friction coefficient and TiO_2/Al_2O_3 nanolaminate presented the lowest friction reduction when compared with the bare Ti-6Al-4V sample. Analyzing tribocorrosion and adherence results, it can be concluded that these films are indicated for use in devices operating at fixed positions or for low load applications, as example in the case of the dispositive used for implanted sensors in the body.

Acknowledgements

This study was supported by the Fundação de Amparo à Pesquisa do Estado de São Paulo (FAPESP) Project numbers (2003/13373-8, 2004/10856-0, 2008/05533-9 and 2011/50773-0) Conselho Nacional de Desenvolvimento Científico e Tecnológico (CNPq) Project number (313280/2014-2), and by the Coordenação de Aperfeiçoamento de Pessoal de Nível Superior (CAPES) Project number 005/2014 Capes/ITA. We thank Karina Faria Nass from Instituto Nacional de Pesquisas Espaciais – INPE for indentation analysis and Newton Kiyoshi Fukumasu from Department of Mechanical Engineering, Polytechnic School – University of Sao Paulo – Brasil for nanohardness analysis.

References

[1] U. Kamachimudali, T.M. Sridhar, B. Raj, Corrosion of bio implants, Sadhana 28 (2003) 601–637, http://dx.doi.org/10.1007/BF02706450.
[2] N.D. Nam, S.H. Lee, J.G. Kim, J.W. Yi, K.R. Lee, Effect of stress on the passivation of Si-DLC coating as stent materials in simulated body environment, Diam. Relat. Mater. 18 (2009) 1145–1151, http://dx.doi.org/10.1016/j.diamond.2009.02.032.
[3] S. Bauer, P. Schmuki, K. von der Mark, J. Park, Engineering biocompatible implant surfaces. Part I: materials and surfaces, Prog. Mater. Sci. 58 (2012) 261–326, http://dx.doi.org/10.1016/j.pmatsci.2012.09.001.
[4] Y. Guo, D. Chen, M. Cheng, W. Lu, L. Wang, X. Zhang, The bone tissue compatibility of a new Ti35Nb2Ta3Zr alloy with a low Young's modulus, Int. J. Mol. Med. 31 (2013) 689–697, http://dx.doi.org/10.3892/ijmm.2013.1249.
[5] D. Landolt, Corrosion and Surface Chemistry of Metals, 1st ed., EPFL Press, Lausanne, 2007, http://dx.doi.org/10.1016/S1369-7021(07)70081-0.
[6] ASTM G119-93, Standard guide for determining synergism between wear and corrosion, wear erosion, Met. Corros, 93 1994, pp. 1–7, , http://dx.doi.org/10.1520/G0119-09.2.
[7] M. Li, Y. Cheng, Y.F. Zheng, X. Zhang, T.F. Xi, S.C. Wei, Surface characteristics and corrosion behaviour of WE43 magnesium alloy coated by SiC film, Appl. Surf. Sci. 258 (2012) 3074–3081, http://dx.doi.org/10.1016/j.apsusc.2011.11.040.
[8] S. Mischler, Triboelectrochemical techniques and interpretation methods in tribocorrosion: a comparative evaluation, Tribol. Int. 41 (2008) 573–583, http://dx.doi.org/10.1016/j.triboint.2007.11.003.
[9] P. Ponthiaux, F. Wenger, D. Drees, J.P. Celis, Electrochemical techniques for studying tribocorrosion processes, Wear 256 (2004) 459–468, http://dx.doi.org/10.1016/S0043-1648(03)00556-8.
[10] A.A. Voevodin, J.S. Zabinski, Nanocomposite and nanostructured tribological materials for space applications, Compos. Sci. Technol. 65 (2005) 741–748, http://dx.doi.org/10.1016/j.compscitech.2004.10.008.
[11] C. Fleck, D. Eifler, Corrosion, fatigue and corrosion fatigue behaviour of metal implant materials, especially titanium alloys, Int. J. Fatigue 32 (2010) 929–935, http://dx.doi.org/10.1016/j.ijfatigue.2009.09.009.
[12] R.W.-W. Hsu, C.-C. Yang, C.-A. Huang, Y.-S. Chen, Electrochemical corrosion properties of Ti–6Al–4V implant alloy in the biological environment, Mater. Sci. Eng. A 380 (2004) 100–109, http://dx.doi.org/10.1016/j.msea.2004.03.069.
[13] R.W. Johnson, A. Hultqvist, S.F. Bent, A brief review of atomic layer deposition: from fundamentals to applications, Mater. Today 17 (2014) 236–246, http://dx.doi.org/10.1016/j.mattod.2014.04.026.
[14] F. de P. Santos, E. De Campos, M. Costa, F.C.L. Melo, R.Y. Honda, R.P. Mota, Superficial modifications in TiO_2 and Al_2O_3 ceramics, Mater. Res. 6 (2003) 353–357, http://dx.doi.org/10.1590/S1516-14392003000300009.
[15] G.E. Testoni, W. Chiappim, R.S. Pessoa, M.A. Fraga, W. Miyakawa, K.K. Sakane, et al., Influence of the Al_2O_3 partial-monolayer number on the crystallization mechanism of TiO_2 in ALD TiO_2/Al_2O_3 nanolaminates and its impact on the material properties, J. Phys. D. Appl. Phys. 49 (2016) 375301, , http://dx.doi.org/10.1088/0022-3727/49/37/375301.
[16] M.A. Eckert, P.Q. Vu, K. Zhang, D. Kang, M. Monsur Ali, C. Xu, et al., Novel molecular and nanosensors for in vivo sensing, Theranostics 3 (2013) 583–594, http://dx.doi.org/10.7150/thno.6584.
[17] E. Cianci, S. Lattanzio, G. Seguini, S. Vassanelli, M. Fanciulli, Atomic layer deposited TiO_2 for implantable brain-chip interfacing devices, Thin Solid Films 520 (2012) 4745–4748, http://dx.doi.org/10.1016/j.tsf.2011.10.197.
[18] W. Chiappim, G.E. Testoni, J.S.B. de Lima, H.S. Medeiros, R.S. Pessoa, K.G. Grigorov, et al., Effect of process temperature and reaction cycle number on atomic layer deposition of TiO_2 thin films using $TiCl_4$ and H_2O precursors: correlation between material properties and process environment, Braz. J. Phys. 46 (2016) 56–69, http://dx.doi.org/10.1007/s13538-015-0383-2.
[19] A. C1624-05, Standard Test Method for Adhesion Strength and Mechanical Failure Modes of, 2012 ASTM Int. C1624-5, 2015, pp. 1–29, http://dx.doi.org/10.1520/C1624-05R10.
[20] N. Vidakis, A. Antoniadis, N. Bilalis, The VDI 3198 indentation test evaluation of a reliable qualitative control for layered compounds, J. Mater. Process. Technol. 143–144 (2003) 481–485, http://dx.doi.org/10.1016/S0924-0136(03)00300-5.
[21] L. Vieira, F.L.C. Lucas, S.F. Fisssmer, L.C.D. dos Santos, M. Massi, P.M.S.C.M. Leite, et al., Scratch testing for micro- and nanoscale evaluation of tribocharging in DLC films containing silver nanoparticles using AFM and KPFM techniques, Surf. Coat. Technol. 260 (2014) 205–213, http://dx.doi.org/10.1016/j.surfcoat.2014.06.065.
[22] K.C.F. Nass, P.A. Radi, D.M.G. Leite, M. Massi, A.S. da Silva Sobrinho, R.C.L. Dutra, et al., Tribomechanical and structural properties of a-SiC:H films deposited using liquid precursors on titanium alloy, Surf. Coat. Technol. 284 (2015) 240–246, http://dx.doi.org/10.1016/j.surfcoat.2015.06.080.
[23] H. Zaidi, A. Djamai, K.J. Chin, T. Mathia, Characterisation of DLC coating adherence by scratch testing, Tribol. Int. 39 (2006) 124–128, http://dx.doi.org/10.1016/j.triboint.2005.04.016.
[24] W.C. Oliver, G.M. Pharr, Measurement of hardness and elastic modulus by instrumented indentation: advances in understanding and refinements to methodology, J. Mater. Res. 19 (2004) 3–20, http://dx.doi.org/10.1557/jmr.2004.19.1.3.
[25] Y.S. Jimenez, M.T. Gil, M.T. Guerra, L.S. Baltes, J.C.M. Rosca, Interpretation of Open Circuit Potential of Two Titanium Alloys for a Long Time Immersion in Physiological Fluid, Transilv. Univ. Brasov, 2009, pp. 197–204.
[26] ASTM G3-14, Standard Practice for Conventions Applicable to Electrochemical Measurements, ASTM Stand. 03.02, 2014, pp. 1–9, http://dx.doi.org/10.1520/G0003-14.
[27] I.E. Wachs, Raman and IR studies of surface metal oxide species on oxide supports: supported metal oxide catalysts, Catal. Today 27 (1996) 437–455, http://dx.doi.org/10.1016/0920-5861(95)00203-0.
[28] C.T. Wang, A. Escudeiro, T. Polcar, A. Cavaleiro, R.J.K. Wood, N. Gao, et al., Indentation and scratch testing of DLC-Zr coatings on ultrafine-grained titanium processed by high-pressure torsion, Wear 306 (2013) 304–310, http://dx.doi.org/10.1016/j.wear.2012.12.033.
[29] A.C. Vieira, A.R. Ribeiro, L.A. Rocha, J.P. Celis, Influence of pH and corrosion inhibitors on the tribocorrosion of titanium in artificial saliva, Wear 261 (2006) 994–1001, http://dx.doi.org/10.1016/j.wear.2006.03.031.